

Raman-shifted Eye-safe Aerosol Lidar (REAL) in 2010: Instrument Status and Two-component Wind Measurements

Shane D. Mayor

Department of Physics
California State University Chico
Chico, California, 95929 USA

ABSTRACT

This paper and corresponding seminar given on 20 September 2010 at the 16th International School for Quantum Electronics in Nesebar, Bulgaria, will describe the key hardware aspects of the Raman-shifted Eye-safe Aerosol Lidar (REAL) and recent advances in extracting two-component wind vector fields from the images it produces. The REAL is an eye-safe, ground-based, scanning, elastic aerosol backscatter lidar operating at 1.54 microns wavelength. Operation at this wavelength offers several advantages compared to other laser wavelengths including: (1) maximum eye-safety, (2) invisible beam, (3) superior performance photodetectors compared with those used at longer wavelengths, (4) low atmospheric molecular scattering when compared with operation at shorter wavelengths, (5) good aerosol backscattering, (6) atmospheric transparency, and (7) availability of optical and photonic components used in the modern telecommunications industry. A key issue for creating a high-performance direct-detection lidar at 1.5 microns is the use of InGaAs avalanche photodetectors that have active areas of at most 200 microns in diameter. The small active area imposes a maximum limitation on the field-of-view of the receiver (about 0.54 mrad full-angle for REAL). As a result, a key requirement is a transmitter that can produce a pulsed (>10 Hz) beam with low divergence (<0.25 mrad full-angle), high pulse-energy (>150 mJ), and short pulse-duration (<10 ns). The REAL achieves this by use of a commercially-available flashlamp-pumped Nd:YAG laser and a custom high-pressure methane gas cell for wavelength shifting via stimulated Raman scattering. The atmospheric aerosol features in the images that REAL produces can be tracked to infer horizontal wind vectors. The method of tracking macroscopic aerosol features has an advantage over Doppler lidars in that two components of motion can be sensed. (Doppler lidars can sense only the radial component of flow.) Two-component velocity estimation is done by computing two-dimensional cross-correlation functions (CCFs) and noting the displacement of the peak of the CCF with respect to the origin. Motion vectors derived from this method are compared with coincident sonic anemometer measurements at 1.6 km range. Preliminary results indicate the method performs best when the atmosphere is stable with light winds.

Keywords: lidar, aerosol, wind, atmosphere

1. BACKGROUND AND RECENT EVENTS

The Raman-shifted Eye-safe Aerosol Lidar (REAL, <http://phys.csuchico.edu/lidar>) is an elastic backscatter aerosol lidar operating at a wavelength of 1.54 microns. It was developed at the National Center for Atmospheric Research (NCAR) between 2001 and 2007 and was moved to California State University Chico in 2008.¹ Figure 1 shows a photograph of the instrument located at the university's 800-acre Agricultural Teaching and Research Center (ATRC). The instrument was moved from the older shipping container on the left to the newer container on the right in 2009.² Previous field deployments of the instrument (Pentagon Shield,³ T-REX,⁴ CHATS,⁵ as examples) were conducted with the instrument housed in the older container which had several problems including sources of dust, leaks, and lack of space. The new container is a custom optical laboratory designed specifically for field deployment of a scanning lidar. It features a substantially improved interior environment for the instrument including a spacious optical table (4.3 m long by 1.2 m wide and 0.45 m thick) and an air conditioning system that uses an exterior heat exchanger in order to eliminate air exchange with the outdoors. This greatly reduces contamination of the interior from dust and insects. An IQ-Air Health Pro Plus HEPA

Author e-mail: sdmayor@csuchico.edu



Figure 1. Raman-shifted Eye-safe Aerosol Lidar (REAL) in Chico, California.

filter continuously purges the laser transmitter area with clean air. The beam-steering unit is attached to the top of a tower made from X-rail and is bolted to the top of the optical table. A neoprene skirt seals the small gap between the flange of the BSU and the roof of the container. Therefore, all optical components of the lidar system are rigidly connected and independent from the container except where the legs of the table are bolted to the floor. The walls and roof of the container are reinforced and insulated. The optical table may be set to float on a pneumatic system to protect the optical components from mechanical shock and vibration during shipment. The containers sit on top of a 48-foot long air-ride trailer with a flat deck. The trailer is composed of steel and wood and considerably heavier than most modern aluminum trailers that have arched decks for heavy loads. The heavy flat-deck trailer was selected as part of an effort to provide a smooth ride for the relatively lightweight containers and contents.

Several journal articles^{6–8} describe the key engineering achievements that enable the high performance, reliability, and eye-safety of the REAL. Many atmospheric lidars exist and many are eye-safe—for example, micropulse lidars⁹ and most heterodyne Doppler lidars.¹⁰ Several other research groups have demonstrated direct-detection lidar at 1.5 microns wavelength.^{11,12} But, the REAL appears to be unique in that the components and configuration of hardware are suitable for ground-based scanning and it has been reproduced several times by a defense contractor for federal government applications. The REALs made by ITT Corp. are used in aerosol plume detection applications¹³ that require scanning, long-range, eye-safety, sensitivity, and continuous and unattended operation. Furthermore, under funding from the U.S. National Science Foundation, algorithms are currently being applied to REAL data in order to derive two-component vector fields of air motion. Preliminary results from this effort are discussed in section 4. But, this article will first describe the key design issues that enable the REAL to perform as well as it currently does.

2. KEY REQUIREMENTS

2.1 Eye-safety

Eye-safety is a non-negotiable requirement for lidar systems that must be used in populated areas and can be achieved by reducing the pulse energy, increasing the transmitted beam diameter, and operating in wavelength regions that have higher maximum eye-safe energy (MEE). Figure 2, reproduced from Spuler and Mayor,¹⁴ shows the MEE versus wavelength as calculated by American National Standard for Safe Use of Lasers, ANSI Z136.1-2000,¹⁵ for single pulse (solid line) and multi-pulse (dashed line) exposures. While no wavelength is inherently eye-safe, some regions of the spectrum offer much higher MEE than others. The 1.5–1.8 micron region offers the highest MEE of any region in the spectrum. REAL operates at 1.54 microns in order to take advantage of this.

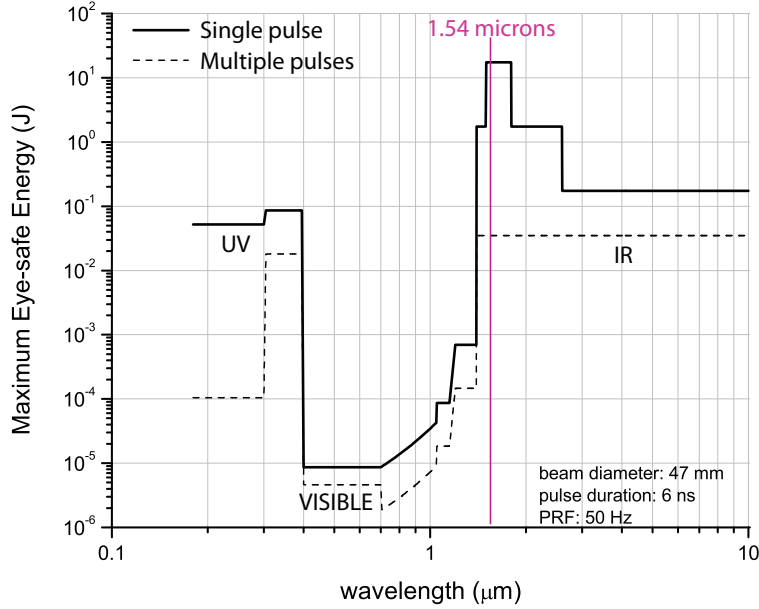


Figure 2. Reproduced from Spuler and Mayor, 2007.¹⁴ Maximum eye-safe energy versus wavelength as calculated by American National Standard for Safe Use of Lasers, ANSI Z136.1-2000, for the conditions shown. The solid curve is calculated for a single shot exposure. The dashed curve is calculated for multiple shots, or stationary laser beam conditions, with exposure times based on the natural aversion time of the human eye: 0.25 s and 10 s for inside and outside the visible wavelength region, respectively.

2.2 Full overlap

A very important design requirement for any atmospheric lidar is that the receiver field of view (FOV) completely surround, or *overlap*, the laser beam as shown in the top diagram in Fig. 3. The bottom diagram in Fig. 3 shows the result when the laser beam is too divergent: it illuminates regions of the atmosphere that the receiver cannot see. Not only is such an arrangement wasteful of the transmitted energy, it creates an additional problem of needing to determine an overlap function that is necessary to eliminate the one-over-range-squared dependence that is inherent in any direct-detection backscatter lidar signal. With full overlap, as shown in the top diagram, the overlap function rapidly increases to, and remains at, one with increasing range. We have found with REAL, where the transmitter and receiver do not share the telescope, that it is most practical to have the receiver FOV at least twice as divergent as the laser beam. This makes it easier in practice to locate and achieve full overlap. The transmit beam is directed up and into the beam steering unit by a 4-inch by 5.6-inch diameter elliptical mirror that is positioned in the shadow of the telescope's secondary mirror. This "launch mirror" is on a piezo-electric tip-tilt stage. Therefore, the transmit beam can be electronically scanned within the receiver's FOV to insure that it indeed within it.

Full overlap can be achieved by reducing the laser beam divergence or increasing the receiver FOV. The receiver FOV can be maximized during design with custom optics, however it will be limited by the diameter of the active area of the photodetector. Large diameter detectors allow for large FOVs and small diameter detectors restrict the FOV. For REAL, we found InGaAs avalanche photodetectors (APDs) have significantly better performance than InGaAs PINs. Unfortunately, InGaAs APDs have small active areas (200 microns diameter at most) thereby restricting the FOV. As a result, a challenge in creating REAL was to identify a laser that could generate pulsed laser radiation in the 1.5–1.8 micron region with sufficiently low divergence. Use of optical parametric oscillators (OPOs) was explored, but it was concluded that the divergence could not be reduced sufficiently, even with beam expansion, to be less than what could practically be achieved for the receiver FOV.¹⁶ Therefore, a commercially available Nd:YAG laser was used with a custom gas wavelength converter. This combination of pump and wavelength converter is described in detail by Spuler and Mayor (2007).¹⁴ Alternative approaches that also capitalize on stimulated Raman scattering in methane are described by Hooper et al.¹⁷ and Trickl.¹⁸

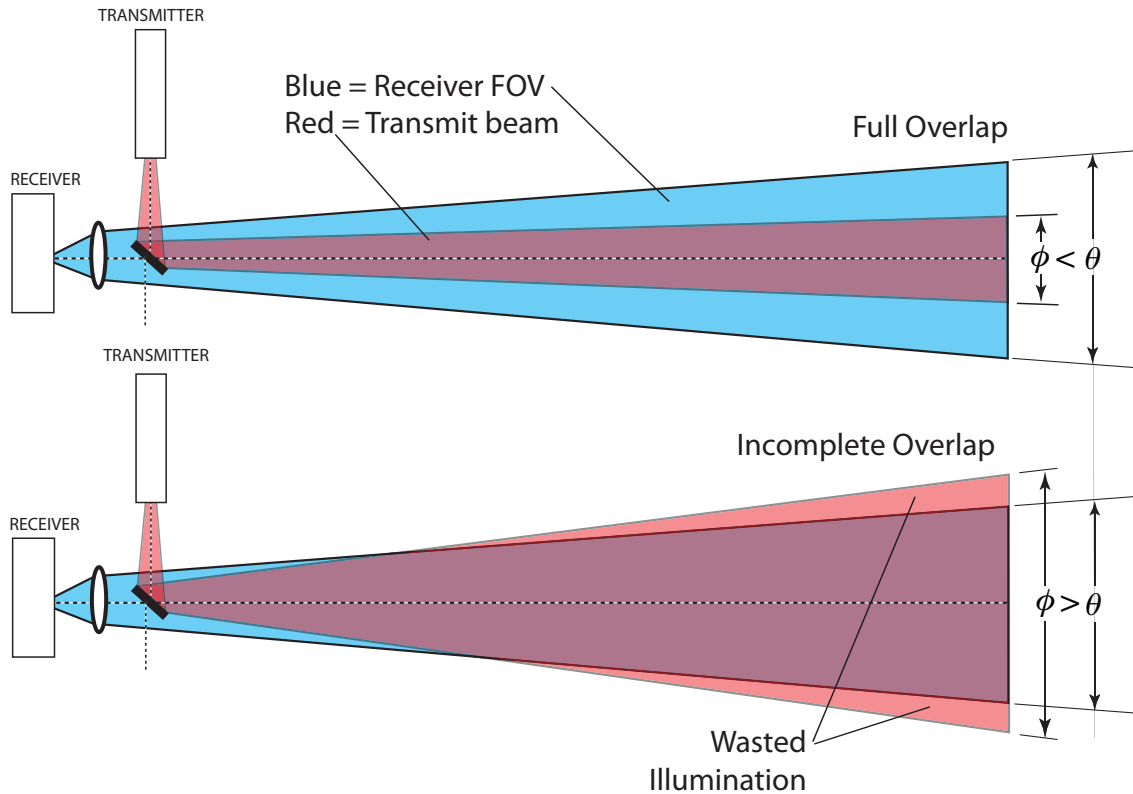


Figure 3. Examples of proper overlap (top) and incomplete overlap (bottom) for an atmospheric lidar system.

The REAL transmitter begins with a commercially available, flashlamp pumped, Nd:YAG laser (a Continuum Surelite III). It produces approximately 800 mJ of laser radiation at 1064 nm at 10 Hz pulse repetition frequency. The pump beam is directed through an optical isolator and a beam reducer before being directed into the Raman cell. Although the beam is weakly convergent in the cell, it is not focused in the cell. Focusing the pump beam results in the breakdown of the gas medium and sooting on the cell windows. In addition to the high energy pump beam, a continuous-wave injection seed beam is directed into Raman cell. The wavelength of the seed beam is at the first Stokes line resulting from stimulated Raman scattering of 1.064 radiation in methane of 1.54 microns. The cell is pressurized with 9.5 atm of methane and 4.1 atm of argon. The argon serves as a buffer gas. Four prisms are used in the cell for 5 passes of the beam. Surfaces of the prisms, and windows of the cell, are oriented at the Brewster angle to minimize reflection without the use of anti-reflection (AR) coatings. The use of prisms instead of mirrors allows avoidance of high reflection (HR) coatings. We found the AR and HR coatings to be a point of weakness in earlier designs. Tiny foreign particles on the surfaces or hot-spots in the beam could cause the coatings at those points to fail.

The design of the wavelength converter in the REAL transmitter has received significant attention. In addition to the coating-free windows and prisms, a series of 8 axial fans circulate the gas and push it through the beam plane. This moves thermal blooms—that would otherwise result in slight variations in the beam pointing direction, lower divergence, and poorer beam quality—out of the way. Downstream of the Raman cell, a prism is used to separate the residual 1.064 micron pump beam from the first Stokes beam at 1.54 microns. The pump beam is stopped by a beam dump while the Stokes beam is expanded in diameter and directed over to the launch mirror. The divergence of the transmit beam can be adjusted by changing the distance between the two lenses of the beam expander.

We found through many hours of experience of using the REAL transmitter in a field environment that key factors for consistent performance include maintaining constant temperature and clean air. These factors are in general not a problem for laboratories in buildings but can become significant in mobile housings where it

Wavelength	1.543 microns
Pulse energy	170 mJ
Pulse rate	10 Hz
Pulse duration	6 ns
Beam diameter at BSU	66 mm ($1/e^2$ points)
Beam divergence	0.12 mrad (half-angle)
Telescope dia.	40 cm
Receiver FOV	0.54 mrad
Digitizer speed	100 MHz
Digitizer range	14 bits
Detector type	200- μ m InGaAs APD

Table 1. REAL System Parameters.

becomes more difficult to control air temperature and dust. For the 2007 CHATS deployment⁵ we made several improvements to the system that allowed us to monitor several performance variables and adjust them remotely. Details of this are described in Section 3.2.

2.3 High Signal-to-Noise Ratio

An important capability of the REAL is its ability to produce high signal-to-noise ratio (SNR) backscatter returns very quickly. This is tantamount to good sensitivity to small changes in aerosol properties such as particle concentration or size distribution. The ability to do this quickly is important because the instrument is scanning and continuously looking at different locations in the atmosphere. Because the spatial distribution of aerosol is moving due to the wind and turbulence, the scans must be collected quickly (<30 s, preferably < 15 s). Averaging backscatter returns from multiple pulses to improve SNR would have an undesirable spatial averaging effect that would reduce the angular resolution of the data. Therefore, REAL combines strong laser pulse energy (170 mJ) with large diameter (40 cm) optics and detection subsystems with large specific detectivity (D^*) to generate high SNR returns from single pulses. In horizontal scan data collected during the CHATS experiment, the backscatter SNR was usually >100 (often 500–1000) at ranges <1 km and remained >10 to ranges of 4–5 km.

2.4 Beam Steering Unit

Another key component of the REAL is the beam steering unit (BSU). Projection of the 40-cm diameter telescope aperture on to surfaces that are always oriented at 45-degrees results in a requirement for mirrors that must have clear reflective areas of at least 40 by 60 cm. Furthermore, because the mirror surfaces project both the transmitted beam and the backscattered radiation, they have flatness requirements on the order of 3-waves over the entire clear aperture. Therefore, care must be taken to use mirrors that will remain sufficiently flat. When the REAL BSU was created in early 2004 (for the Pentagon Shield experiment), time and budget constraints led to the creation of custom “composite mirrors” consisting of 1-inch thick Zerodur glued to 2-inch thick pieces of Hexcel aluminum. This combination resulted in sufficiently lightweight and flat mirror surfaces.⁷ The weight of the mirrors is an important factor because the electrical and mechanical requirements necessary to move the mirrors is proportional. In other words, heavy mirrors require larger and more durable bearings and powerful electric motors. Traditional solid glass mirrors, 3-inches thick, would weigh approximately 120 lbs each. Given the need for repeated rapid accelerations of the mirrors in order to make atmospheric scans there is substantial advantage to having lightweight mirrors. For maximum reflectivity at a broad range of wavelengths,* the mirrors were coated with protected gold. It was noted early on that the “protection” layer over the gold did not offer much protection. As a result, the mirrors were rarely cleaned and became dirty over time.

In April of 2010, the author applied a commercially-available polymer cleaning product to the BSU mirrors. Per instructions, the product was sprayed on, left to dry, and then peeled off. Unfortunately, the author did not test the product on a small section of one mirror or have a witness sample and instead applied the product to the entire surfaces of both mirrors. Peeling the product off resulted in partial removal of the gold coatings. As a

*Initially, it was not known whether the BSU would be used at only 1.5 microns.

result of this accident, new BSU mirrors with a honeycomb internal structure for lightness and durable enhanced aluminum coatings for the specific wavelength of REAL are being fabricated at the time of this writing. Delivery of the new mirrors is expected in early 2011.

3. OTHER USEFUL CAPABILITIES

3.1 Polarization Sensitivity

In 2005, backscatter depolarization sensitivity was added to the REAL. It was done by improving the linear polarization purity of the transmitter and adding a polarization rotator, polarization beam splitter cube and second detection channel in the receiver. Details of the upgrades and results of field testing are described in Mayor et al.⁸ To summarize, the REAL transmitter is now capable of producing linearly polarized laser radiation with a 10,000:1 purity. Unfortunately, due to the angle that the beam is projected on to the launch mirror, it was (and remains) likely not linearly polarized upon entering the BSU. Furthermore, when the BSU is not directed horizontally, differential phase delay from the BSU mirrors results in a systematic error of the depolarization ratio that is a function of azimuth and elevation angle. As a result, the backscatter depolarization ratios are not absolute. The polarization characteristics of the beam exiting the BSU were not measured. In the future this should be done with a polarimeter.

The above however is not to say that the backscatter depolarization ratios do not have value. As shown in Mayor et al.,⁸ the system shows a very clear difference in depolarization ratios between controlled wet and dry aerosol plumes near the ground. Similar changes in backscatter depolarization ratio have been observed in water clouds aloft. In the future, opto-mechanical components could be added to the system to rotate the polarization vector to maintain a beam with constant linear polarization in the atmosphere.

3.2 Continuous and Unattended Operation

Recognizing the expense and inconvenience of requiring a person to be present at the lidar in order to operate it, software and hardware was added to the REAL in late 2006 and early 2007, just prior to CHATS,⁵ to enable nearly continuous and unattended operation.¹⁹ The most significant of the hardware additions was a laser beam profiling system. The CCD camera of the beam profiler was positioned to intercept the 1064 nm pump beam leakage through a 45-degree turning mirror after the Raman-cell. The beam profiler CCD camera was connected to a Windows PC that was connected to a network in the lidar container. Beam profiler software installed on the PC enabled continuous monitoring of the position, diameter, and shape of the pump beam. The beam profiler software recorded these characteristics so that we could see trends or identify problems. In addition, several air temperature sensors were installed and interfaced with the lidar's data acquisition system. The data acquisition software, written in Labview, was modified to record pump laser pulse energy, Stokes pulse energy, temperatures of the Raman cell and indoor air, and Raman cell gas pressure in an ASCII data file once per minute. Results are shown in Fig. 4. In addition, the data acquisition software was modified to communicate with the Stokes injection seed and Nd:YAG lasers. RealVNC® software was installed on both computers that were connected to a network hub and an internet connection. This provided us with remote desktop control of the two computers from other locations. During CHATS, that took place in Dixon, California, we monitored the system through the internet connection from Boulder, Colorado. Several visits were made to the lidar during the three month period to restart electrical devices that shut off due to power interruptions. However, during CHATS, about 1850 hours of data were collected, an 85 percent "up-time". Typically, we logged into the REAL computers once or twice a day to check the system status. Occasionally, we increased the flash-lamp voltage through the remote computer control of the Nd:YAG laser.

In addition to remote control, the data acquisition software, which also sends instructions and receives data from the BSU, was modified so that sequences of different types of scans could be performed. For example, a common scan strategy at CHATS was to repeatedly collect one PPI and one RHI so that both horizontal and vertical cross-sectional animations of the atmosphere could be obtained. The complete set of REAL scans in the form of images and animations can be obtained on line at <http://phys.csuchico.edu/lidar>.

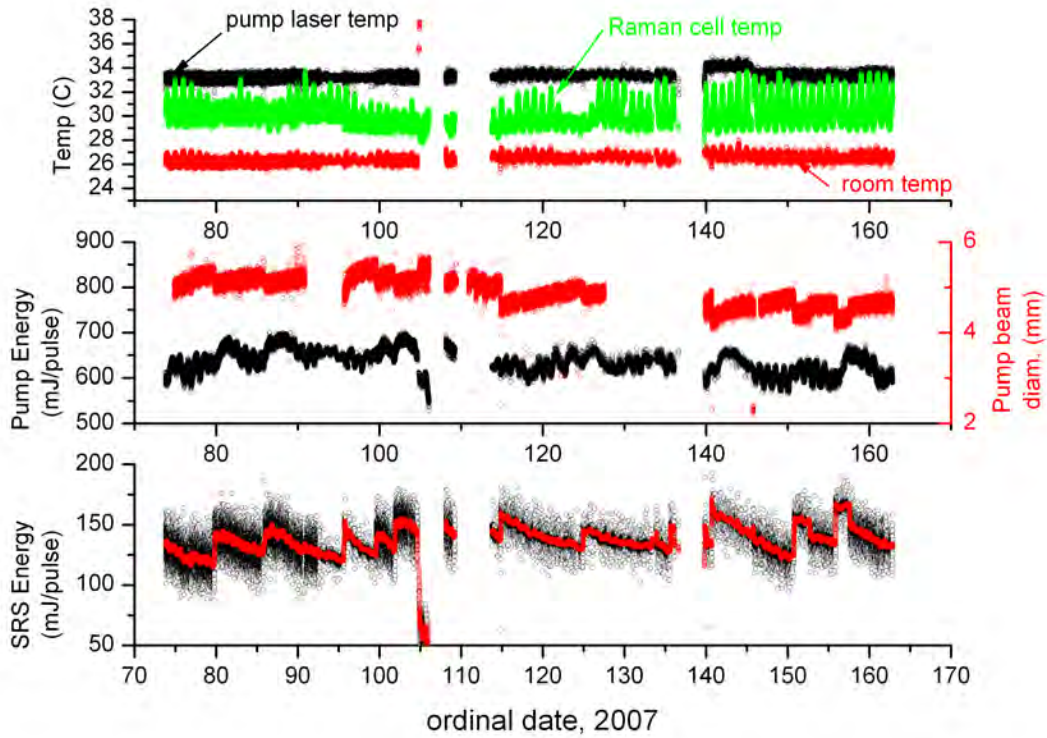


Figure 4. Time series of variables associated with the REAL transmitter during the three-month CHATS deployment.

4. WIND MEASUREMENT

Remote measurement of the wind continues to be a need in several areas including security,¹³ transportation,²⁰ wind energy,²¹ and meteorology.²² Doppler lidars are designed to measure the wind.^{10,23,24} A vibrant Doppler lidar community exists and Doppler lidars have been commercially available for some time. The fundamental method of Doppler lidar is to measure the frequency shift of the backscattered laser radiation due to the wind induced motion of the scatterers. Air motion of course is three dimensional and Doppler lidars are only capable of sensing the component of motion along the laser beam's line-of-sight. In other words, only the component of motion directly toward or away from the lidar. This is called the *radial* component because lidars (and radars) make observations in a spherical coordinate system (azimuth, elevation, and range). The other components of motion, the *tangential* components (flow across the beam) are not detected by Doppler lidars. To compensate for this fundamental limitation, Doppler lidars are often scanned and an assumption of horizontally homogeneous flow is usually invoked in order to infer two wind components.[†] In summary, the radial components measured by Doppler lidar may have very high spatial and temporal resolution and accuracy, but after scanning and assuming horizontally homogeneous flow, the resolution and accuracy of multi-component wind measurements may be comparatively poor. Furthermore, in many applications it is not practical to collect 360-degree scans and the horizontally homogeneous flow assumption may not be valid.

An alternative method to measure two (or possibly three in the future) components of the wind remotely is

[†]Two Doppler lidars have been used to scan over a common area to obtain two components of flow. And radial velocities have been fed into numerical models in order to obtain additional components. These methods are valid, but ultimately one lidar is providing one velocity component. My goal is to measure two velocity components from a single instrument with resolution and accuracy exceeding those achieved by the use of current Doppler lidar(s) and any assumptions about the flow.

by use of either cross-correlation^{25,26} or optical flow algorithms.²⁶⁻²⁹ In this paper, I will focus on the results of the cross-correlation method. These results were also recently presented at the 25th International Laser Radar Conference.²⁵ The reader is referred to the conference paper by Dérian et al.²⁹ for results of the application of dense estimation optical flow to the same REAL data.

The cross-correlation technique has been applied to aerosol lidar data several times previously.³⁰⁻³⁷ It was also applied to weather radar data³⁸ and satellite images.³⁹ The most recent of these papers³⁷ showed two-component vector fields with 250 m horizontal resolution over areas as large as 60 km². These vectors however were the result of large amounts of temporal averaging of many cross-correlation functions—up to 41 minutes in one case—in order to obtain mean properties of an offshore wind field. Furthermore, the lidar used in Mayor and Eloranta³⁷ was not eye-safe and the scans were not coincident with any independent forms of wind measurement for validation. In the present work, no temporal averaging of the cross-correlation functions was performed. Moreover, the following results were collected with an eye-safe system and a micro-meteorological tower was located within the lidar scan plane for validation. This data set enables a comprehensive evaluation of the technique that will be conducted over the next two years under a grant from the U.S. National Science Foundation. Details of the algorithm used are in a paper presented at the 25th International Laser Radar Conference.²⁵ In this paper, just two brief cases are presented. More information on the cases can be found in papers presented at the 24th and 25th ILRCs^{25,40} and a journal article currently in press.⁴¹

4.1 21 March 2007

The first case is from the evening of 21 March 2007 between 04:15 and 06:45 UTC (see Figs. 5 and 6). This 2.5 hour period occurred during the evening from about sunset until 15 minutes before midnight. During this time the atmospheric surface layer was weakly stable (z/L stability parameter at 12.5 m AGL was +0.035) and the winds were light (less than 2 m s⁻¹ for the most part) and variable. The lidar was programmed to repeat a sequence of 40 consecutive PPI scans followed by 2 consecutive RHI scans. The PPI scans ranged from 150° to 210° azimuth at a scan rate of 4° s⁻¹. This resulted in one scan every 17.3 s. The lidar transmitted 10 pulses per s and digitized backscatter at 1.5 m intervals in range. The angular separation between beams was 0.4°.

Motion vectors were calculated from pairs of frames over a 250 m x 250 m area of lidar backscatter data centered on the ISFF vertical tower that was located 1600 m directly south of the lidar site. Fig. 5 shows the u -component (top panel) and v -component (bottom panel) during the period from the lidar (black) and a sonic anemometer (red) from 12.5 m AGL on the tower—the height closest to the lidar scan plane at that range. The sonic anemometer data (sampled at 60 Hz) have been averaged over the time span required by the lidar to scan the 250 m x 250 m region twice. Therefore, data points shown for both the lidar and in situ wind are plotted every 17.3 s. The average SNR of the raw backscatter data over this region ranged from 63 to 166 during the period. The SNR of the images used to compute the cross-correlation functions ranged from 0.43 to 22 and had a median value of 1.8.

Time-lapse animations of the lidar images from this case (21 March) show a what appear to be a substantial amount of gravity wave activity and episodes of turbulence. The gravity wave propagation vector may not equal the local wind vector. A hypothesis of this research was that the correlation technique may fail during stable periods because it may track wave propagation. These results suggest that the correlation method is capable of good performance during weakly stable and light wind conditions with wave activity.

4.2 26 April 2007

The second case is from the afternoon between 22:00 UTC on 26 April and 01:00 UTC on 27 April 2007 (see Figs. 7 and 8). Details of this case, and 6 other density current front cases, can be found in a paper by Mayor.⁴¹ The lidar was programmed to collect alternating RHI and PPI scans. This provided one PPI scan (or one RHI scan) every 30 s. The PPI scans were directed between 151° and 211° azimuth at a scan rate of 4° s⁻¹. As with the previous case, the lidar transmitted 10 pulses per second and digitized backscatter at 1.5 m intervals in range. The angular separation between beams was 0.4°. During this period, a density current front passed over the experimental site at 23:25 UTC on 26 April. The z/L stability parameter at 12.5 m height ranged from -2.0 to -0.6 (strongly to moderately unstable) before the arrival of the front to -0.5 to -0.2 (moderately to weakly unstable) after the passage of the front. During the entire period, wind speeds remained below approximately 4

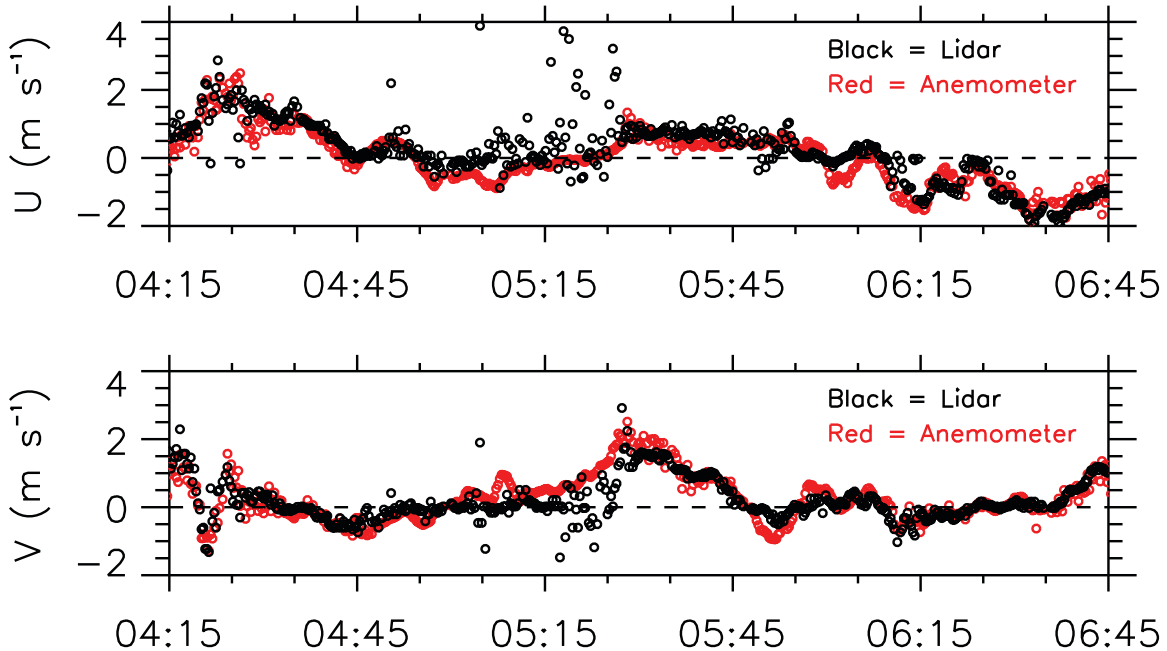


Figure 5. Time series comparison of u (east-west) and v (north-south) components of motion for a 2.5 hour period on the evening of 21 March 2007 when conditions were weakly stable and nearly quiescent. The black data points are from the lidar data and the red data points are from the sonic anemometer. Data points are spaced every 17.3 s.

m s^{-1} . However, the wind direction changed dramatically from 350° (N) before the front to 221° (SSW) after the front. The 26 April case (Fig.7) shows a substantial amount of scatter in both the anemometer wind speeds and the lidar wind speeds that is not present in the previous case. This difference is attributed to the more turbulent, and spatially inhomogeneous velocity field, during that time.

5. CONCLUSIONS

Previous work, nearly 40 years ago,^{30–32} showed the potential of high pulse-energy, ground-based, scanning elastic backscatter lidar to reveal the internal structure and motion of the lower atmosphere. However, it is likely that lack of eye-safety limited further development and widespread use. The 1.5–1.8 micron wavelength region offers orders magnitude more eye-safety than 1064 nm. Therefore, continued development within this wavelength band is likely to result in new active remote sensing capabilities.

My colleagues at NCAR and I found several key requirements that must be met to create a high pulse-energy, direct-detection, elastic backscatter lidar at 1.5 microns. First, use of InGaAs APDs provides the detectivity and responsivity needed for sensing fine-scale aerosol features. (PIN type detectors were not adequate.) The APDs currently available are at most 200 microns in diameter. This small active area subtends a relatively narrow receiver FOV even when maximized using custom optics. We found that a custom triplet focusing lens was required and, when used with a 40 cm diameter $f/3$ Newtonian telescope, yielded a 0.54 mrad FOV. This sets a maximum divergence of the transmitted laser beam. Ideally, the divergence of the transmitted beam should be substantially less for ease of alignment.

During the initial development of REAL, we were not able to find a commercially available laser transmitter that operated between 1.5 and 1.8 microns with sufficient pulse energy, short pulse length and, most importantly, sufficiently low beam divergence. Therefore, we undertook the development of a wavelength converting Raman cell that would not have the traditional problems of previous of Raman cells. The cell we developed featured reasonably sized apertures to ease alignment with a beam that was not very small in diameter or likely to burn the edges of the aperture if slightly misdirected during alignment. The cell windows were oriented at the Brewster angle to eliminate the need for anti-reflection coatings. We used prisms inside the cell for a multi-pass configuration (approximately 3 m interaction path length). The faces of the prisms were also oriented at the

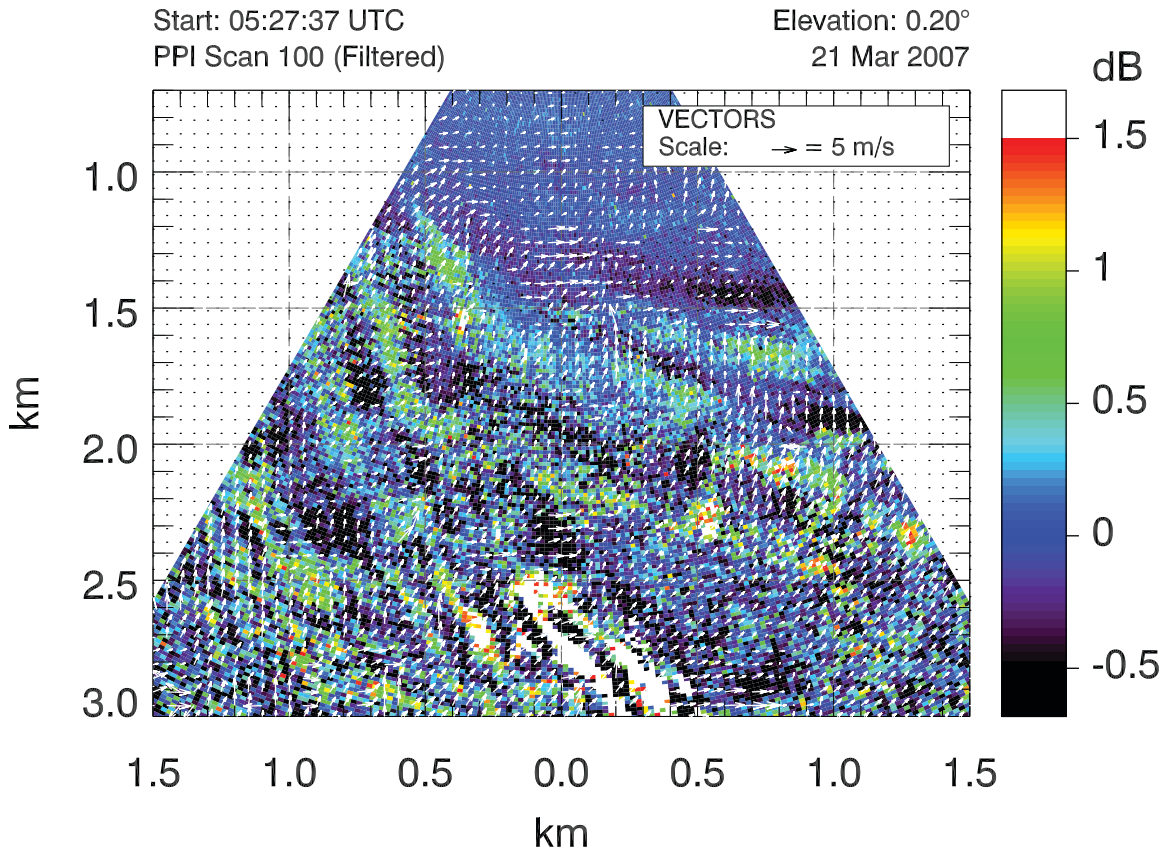


Figure 6. Two component vector flow field for a pair of scans collected on the evening of 21 March 2007. The vectors are spaced every 50 m in x and y and are the result of 250 m x 250 m areas. The vectors are superimposed on one of the two high-pass median filtered backscatter intensity images that were used to compute the vectors.

Brewster angle. This eliminated the need for any AR or HR coatings in the cell. The cell uses a series of axial fans to circulate the CH_4 and Ar gas mixture. Finally, the pump beam is not focused in the cell and the cell is injection seeded at the Stokes wavelength. We found all of these things necessary to reliably convert 1064 nm pump to 1543 nm with reasonable efficiency, beam characteristics, and reliability. If pumped correctly, the cell suffers from no contamination or deterioration over time.

Several other technologies have been key to enabling reliable, unattended, and nearly-continuous operation of the REAL. First, the environment in which the instrument operates must be temperature stabilized and free of dust and insects. Second, laser beam diagnostics that are recorded and are able to be plotted from a remote location to identify problems and trends are critical. For example, a slow and steady decreasing pulse energy is symptom of the natural deterioration of laser flash lamps and must be compensated for periodically by increasing the flash lamp voltage. Therefore, computer control of the pump laser's power and cooling unit is required. Finally, uninterruptable power supplies are very valuable as small inconsistencies in electrical power to the lidar site can cause one or more components to reset and cause a cascade of problems for the entire system.

In terms of wind measurement, preliminary results suggest that agreement of the vectors between correlation method and averaged sonic-anemometer data are best during light wind and stable conditions. High frequency agreement between the two forms of air velocity measurements becomes poorer during windy and turbulent conditions. A comprehensive comparison is currently being conducted. In the future, we plan to compute high resolution vector flow fields in real-time. Such a capability may have value in the short-term prediction of aerosol plume transport and dispersion, for example. Real-time execution means completing all calculations within the time required to perform one scan (typically about 15 s). Therefore, we recently began exploring methods to optimize the execution of the program including multithreading, CPU SIMD instructions, and general purpose

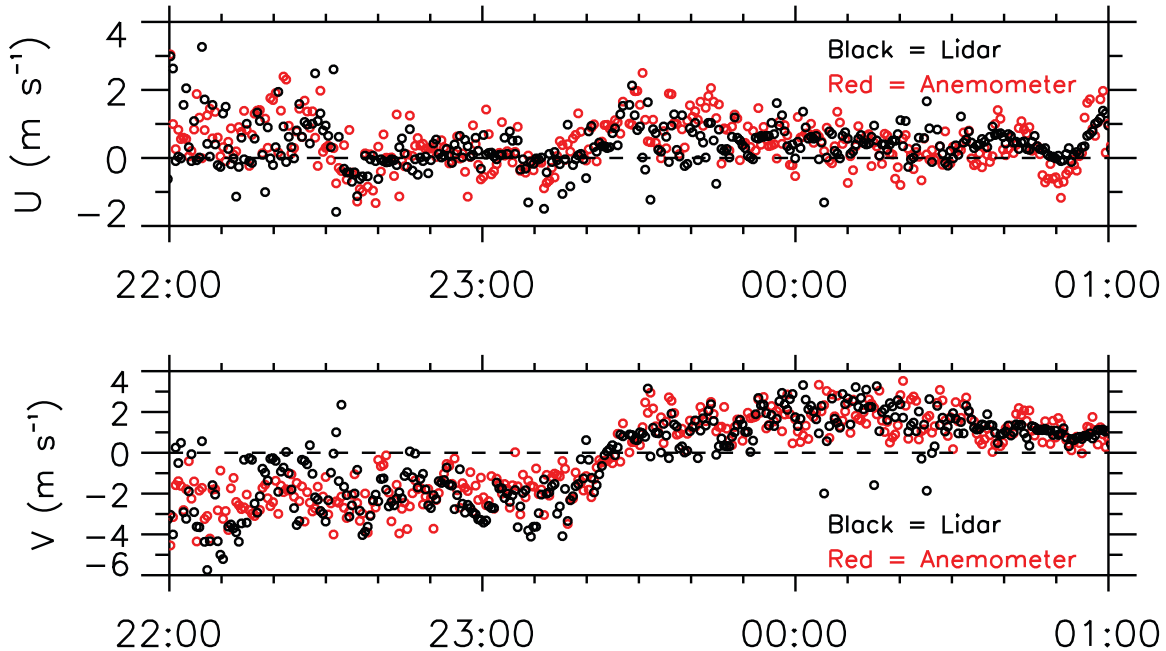


Figure 7. Time series comparison of u (east-west) and v (north-south) components of motion during a 3-hour period on the afternoon of 26 April 2007. During this period, a density current front passed over the site causing a near reversal of the v -component. The atmosphere during this case was unstable and turbulent. The black data points are from the lidar data using a 500 m x 500 m box centered on the ISFF vertical tower and the red data points are from the sonic anemometer on the tower. Data points are spaced every 30 s.

graphics processing units (GPGPU).

ACKNOWLEDGMENTS

REAL was developed at NCAR with funding from the US National Science Foundation. Dr. Scott Spuler and Mr. Bruce Morley developed and deployed the instrument. The recent work of deriving vectors from the CHATS data using the correlation technique and this paper and presentation at the 16th ISQE were made possible by Grant 0924407 from NSF's Physical and Dynamic Meteorology Program.

REFERENCES

- [1] Kintisch, E., "Turbulent times for climate model," *Science* **321**, 1032–1034 (2008).
- [2] McAfee, T. R., Griffo, C. F., Petrova-Mayor, A., and Mayor, S. D., "Rebuilding the Raman-shifted Eye-safe Aerosol Lidar (REAL)," in [*California State University Chico College of Natural Sciences 5th Annual Poster Session*], (2009).
- [3] Warner, T., Benda, P., Swerdlin, S., Knievel, J., Argenta, E., Aronian, B., Balsley, B., Bowers, J., Carter, R., Clark, P. A., Clawson, K., Copeland, J., Crook, A., Frehlich, R., Jensen, M. L., Liu, Y., Mayor, S., Meillier, Y., Morley, B., Sharman, R., Spuler, S., Storwold, D., Sun, J., Weil, J., Xu, M., Yates, A., and Zhang, Y., "The Pentagon Shield Field Program: Toward Critical Infrastructure Protection," *Bull. Amer. Meteor. Soc.* **88**, 167–176 (2007).
- [4] DeWecker, S. F. J. and Mayor, S. D., "Observations of atmospheric structure and dynamics in the Owens Valley of California with a ground-based, eye-safe, scanning aerosol lidar," *J. Clim. Appl. Meteor.* **48**, 1483–1499 (2009).
- [5] Patton, E. G., Horst, T. W., Sullivan, P. P., Lenschow, D. H., Oncley, S. P., Brown, W. O. J., Burns, S. P., Guenther, A. B., Held, A., Karl, T., Mayor, S. D., Rizzo, L. V., Spuler, S. M., Sun, J., Turnipseed, A. A., Allwine, E. J., Edburg, S. L., Lamb, B. K., Avissar, R., Calhoun, R., Kleissl, J., Massman, W. J., U, K.

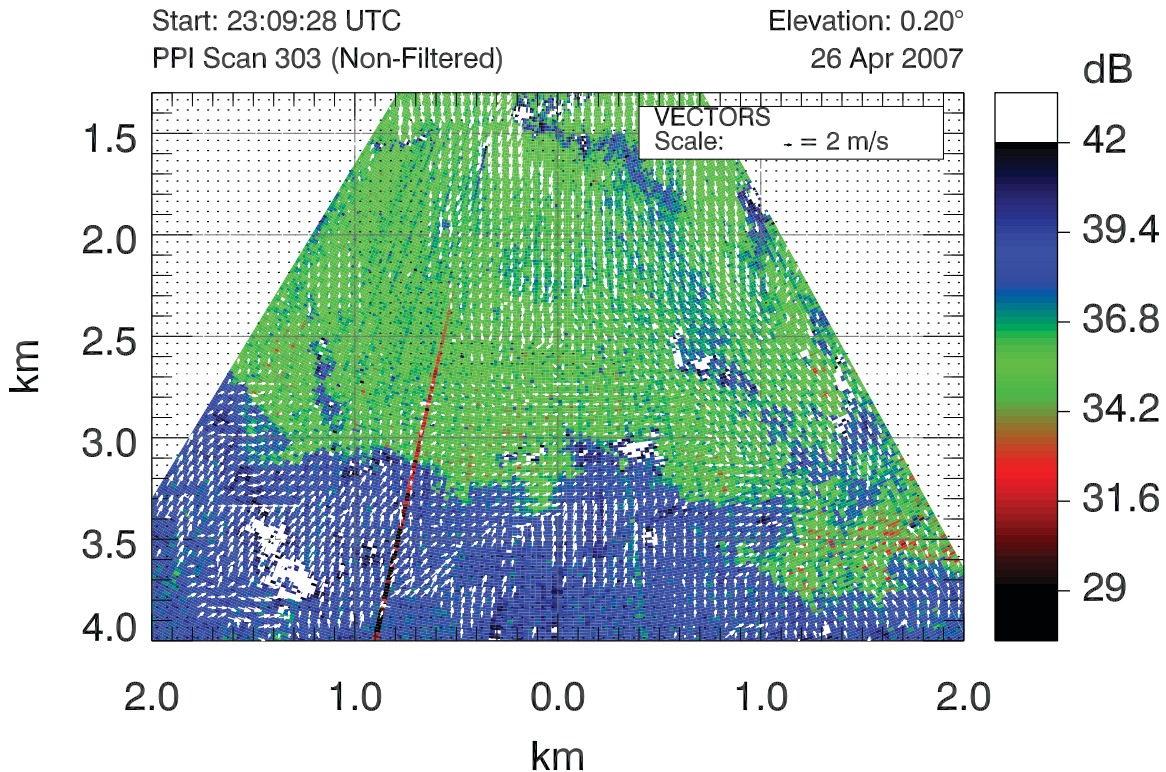


Figure 8. Two component vector flow field for one pair of scans collected on 26 April 2007. The vectors are spaced every 50 m in x and y and are the result of 500 m x 500 m areas. The vectors are superimposed on one of the two high-pass median filtered backscatter intensity images that was used to compute the vectors. The color scale of the backscatter data has been adjusted so that the advancing marine airmass is blue and the airmass north of it is green.

T. P., and Weil, J. C., “The Canopy Horizontal Array Turbulence Study (CHATS),” *Bull. Amer. Meteor. Soc.*, Accepted (2010).

- [6] Mayor, S. D. and Spuler, S. M., “Raman-shifted Eye-safe aerosol lidar (REAL),” *Appl. Optics* **43**, 3915–3924 (2004).
- [7] Spuler, S. M. and Mayor, S. D., “Scanning eye-safe elastic backscatter lidar at 1.54 microns,” *J. Atmos. Ocean. Technol.* **22**, 696–703 (2005).
- [8] Mayor, S. D., Spuler, S. M., Morley, B. M., and Loew, E., “Polarization lidar at 1.54-microns and observations of plumes from aerosol generators,” *Opt. Eng.* **46**, DOI: 10.1117/12.781902 (2007).
- [9] Spinhirne, J. D., “Micro pulse lidar,” *IEEE Trans. Geosci. Remote Sensing* **31**, 48–55 (1993).
- [10] Grund, C. J., Banta, R. M., George, J. L., Howell, J. N., Post, M. J., Richter, R. A., and Weickman, A. M., “High-resolution Doppler lidar for boundary layer and cloud research,” *J. Atmos. Ocean. Technol.* **18**, 376–393 (2001).
- [11] Carnuth, W. and Trickl, T., “A powerful eyesafe infrared aerosol lidar: Application of stimulated raman backscattering of 1.06 micron radiation,” *Rev. Sci. Instrum.* **65**, 3324–3331 (1994).
- [12] Spinhirne, J. D., Chudamani, S., Cavanaugh, J. F., and Bufton, J. L., “Aerosol and cloud backscatter at 1.06, 1.54, and 0.53 μm by airborne hard-target-calibrated Nd : YAG/ methane Raman lidar,” *Appl. Optics* **36**, 3475–3490 (1997).
- [13] Mayor, S. D., Benda, P., Murata, C. E., and Danzig, R. J., “Lidars: A key component of urban biodefense,” *Biosecur. Bioterror.* **6**, 45–56, DOI: 10.1089 bsp.2007.0053 (2008).
- [14] Spuler, S. M. and Mayor, S. D., “Raman shifter optimized for lidar at 1.5-micron wavelength,” *Appl. Optics* **46**, 2990–2995 (2007).
- [15] “American National Standard for Safe Use of Lasers,” Tech. Rep. Z136.1, Laser Institute of America (2000).

- [16] Mamidipudi, P. and Killinger, D., “Optimal detector selection for a 1.5 micron ktp opo atmospheric lidar,” in [*SPIE Conference on Laser Radar Technology and Applications IV*], **3707**, 327–335, SPIE (1999).
- [17] Hooper, W. P., Frick, G. M., and Michael, B. P., “Using backward raman scattering from coupled deuterium cells for wavelength shifting,” *Opt. Eng.* **48**, 084302–1–6 (2009).
- [18] Trickl, T., “Upgraded 1.56 μm lidar at imkifu with 0.28 J/pulse,” *Appl. Optics* **49**, 3732–3740 (2010).
- [19] Spuler, S. M. and Mayor, S. D., “Eye-safe aerosol lidar at 1.5 microns: progress towards a scanning lidar network,” in [*SPIE Lidar Remote Sensing for Environmental Monitoring VIII*], DOI: 10.1117/12.739519 (2007).
- [20] National Academy of Sciences, [*Wake Turbulence: An Obstacle to Increased Air Traffic Capacity*], National Academies Press, 500 Fifth Street, N.W., Washington, DC 20055 (2008).
- [21] “And now, the electricity forecast,” *The Economist Technology Quarterly* **395**(8686), 14–15 (12 June 2010).
- [22] National Academy of Sciences, [*Why Weather Matters: Science and Service to Meet Critical Societal Needs*], National Academies Press, 500 Fifth Street, N.W., Washington, DC 20055 (2010).
- [23] Post, M. J. and Cupp, R. E., “Optimizing a pulsed Doppler lidar,” *Appl. Optics* **29**, 4115–4158 (1990).
- [24] Henderson, S. W., Hale, C. P., Magee, J. R., Kavaya, M. J., and Huffaker, A. V., “Eye-safe coherent laser radar system at 2.1 micron using tm,ho:yag lasers,” *Opt. Lett.* **16**, 773–775 (1991).
- [25] Mayor, S. D., “Horizontal motion vectors from cross-correlation: First application to eye-safe aerosol lidar data from CHATS,” in [*25th International Laser Radar Conference*], (2010).
- [26] Mayor, S. D., Dérian, P., Héas, P., and Mémin, E., “Two-component horizontal motion vectors from scanning eye-safe aerosol lidar,” in [*19th Symp. on Boundary Layers and Turbulence*], AMS (2010).
- [27] Horn, B. K. P. and Schunck, B. G., “Determining optical flow,” *Artificial Intelligence* **17**, 185–203 (1981).
- [28] Corpetti, T., Mémin, E., and Perez, P., “Dense estimation of fluid flows,” *IEEE Trans. Pattern Analysis Machine Intelligence* **24**, 365–380 (2002).
- [29] Dérian, P., Héas, P., Mémin, E., and Mayor, S. D., “Dense motion estimation from eye-safe aerosol lidar data,” in [*25th International Laser Radar Conference*], (2010).
- [30] Eloranta, E. W., King, J. M., and Weinman, J. A., “The determination of wind speeds in the boundary layer by monostatic lidar,” *J. Appl. Meteor.* **14**, 1485–1489 (1975).
- [31] Sroga, J. T., Eloranta, E. W., and Barber, T., “Lidar measurements of wind velocity profiles in the boundary layer,” *J. Appl. Meteor.* **19**, 598–605 (1980).
- [32] Kunkel, K. E., Eloranta, E. W., and Weinman, J., “Remote determination of winds, turbulence spectra and energy dissipation rates in the boundary layer from lidar measurements,” *J. Atmos. Sci.* **37**, 978–985 (1980).
- [33] Sasano, Y., Hirohara, H., Yamasaki, T., Shimizu, H., Takeuchi, N., and Kawamura, T., “Horizontal wind vector determination from the displacement of aerosol distribution patterns observed by a scanning lidar,” *J. Appl. Meteor.* **21**, 1516–1523 (1982).
- [34] Hooper, W. P. and Eloranta, E. W., “Lidar measurements of wind in the planetary boundary layer: the method, accuracy and results from joint measurements with radiosonde and kytoon,” *J. Clim. Appl. Meteor.* **25**, 990–1001 (1986).
- [35] Kolev, I., Parvanov, O., and Kaprielov, B., “Lidar determination of winds by aerosol inhomogeneities: motion velocity in the planetary boundary layer,” *Appl. Optics* **27**, 2524–2531 (1988).
- [36] Schols, J. L. and Eloranta, E. W., “The calculation of area-averaged vertical profiles of the horizontal wind velocity from volume imaging lidar data,” *J. Geophys. Res.* **97**, 18395–18407 (1992).
- [37] Mayor, S. D. and Eloranta, E. W., “Two-dimensional vector wind fields from volume imaging lidar data,” *J. Appl. Meteor.* **40**, 1331–1346 (2001).
- [38] Rinehart, R. E. and Garvey, E. T., “Three-dimensional storm motion detection by conventional weather radar,” *Nature* **273**, 287–289 (1978).
- [39] Leese, J. A., Novak, C. S., and Clark, B. B., “An automated technique for obtaining cloud motion from geosynchronous satellite data using cross correlation,” *J. Appl. Meteor.* **10**, 118–132 (1971).
- [40] Mayor, S. D., “Observations of sea-breeze fronts and turbulence near the surface during stable conditions,” in [*24th International Laser Radar Conference*], SO30–01 (2008).
- [41] Mayor, S. D., “Observations of seven density current fronts in Dixon, California,” *Mon. Wea. Rev.*, In Press (2010).